J Toxicol Pathol 2022; 35: 299–311

Original Article

Changes in 5-Fluorouracil-induced external granular cell damage during the time-course of the developing cerebellum of infant rats

Yuko Yamaguchi[1]*, Tsubasa Saito[1], Mizuho Takagi[1], Tomomi Nakazawa[1], and Kazutoshi Tamura[1]

[1] Pathology Division, Gotemba Laboratories, BoZo Research Center Inc., 1284 Kamado, Gotemba, Shizuoka 412-0039, Japan

Abstract: 5-Fluorouracil (5-FU) is widely used as a chemotherapeutic agent that blocks DNA synthesis and replication by inhibiting thymidylate synthetase. This study aimed to elucidate 5-FU-induced changes in the external granular cells (EGCs) in the cerebellum of infant rats and the possible underlying mechanism. Six-day-old infant rats were injected subcutaneously with 40 mg/kg of 5-FU, and their cerebellums were examined at 6, 9, 12, and 24 h after treatment (HAT), and 2, 4, and 10 d after treatment (DAT). The width of the external granular layer (EGL) decreased from 24 HAT to 4 DAT in the 5-FU group compared to that in the control group. However, the width in the 5-FU group was comparable to that of the control group at 10 DAT. The number of apoptotic cells, cleaved caspase 3-labeling index (LI%), $p21^{cip1}$-LI%, and expression levels of *p53*, *$p21^{cip1}$,* and *Fas* mRNAs increased at 24 HAT. However, no changes were detected in the expression levels of *Puma* and *Bax* mRNAs at any time point. BrdU-LI% increased at 6 and 12 HAT but decreased at 24 HAT. The phospho-histone H3-LI% decreased from 6 HAT to 2 DAT. The width of the molecular layer decreased compared to that of the control group at 10 DAT. No differences were observed in Purkinje cell development. These results indicate that 5-FU inhibited cell proliferation by inducing apoptosis of EGCs via activation of Fas and caspase-3 without the involvement of the mitochondrial pathway and induced p53-dependent G1-S and G2-M phase arrest. (DOI: 10.1293/tox.2022-0003; J Toxicol Pathol 2022; 35: 299–311)

Key words: 5-Fluorouracil, external granular cell, apoptosis, cell cycle arrest, immunohistochemistry, reverse transcription polymerase chain reaction (RT-PCR)

Introduction

As a widely used chemotherapeutic agent, 5-Fluorouracil (5-FU) blocks DNA synthesis and replication via inhibition of thymidylate synthetase (TS) and incorporation of its metabolites into RNA and DNA[1]. 5-FU is absorbed rapidly into the maternal circulation, and its metabolites are directly incorporated into embryonic nucleic acid[2]. Since 5-FU readily crosses the blood-brain barrier (BBB), it induces teratogenic effects and subsequent developmental anomalies in the brain of rodents and humans[3–8]. Moreover, there is some evidence showing that 5-FU can cross the BBB by simple diffusion and exert neurotoxic effects, thereby leading to nystagmus, ataxia, dysarthria, and epilepsy in humans[9, 10]. Although several DNA-damaging agents have demonstrated toxic effects on the developing brains of fetuses and newborns of rats and mice[11], 5-FU has not been adequately investigated for its toxic effects on the developing central nervous system (CNS). Few detailed reports have been published examining the effects and mechanism of DNA-damaging agents[12–17], including 5-FU[18], in the developing cerebellum; however, the timings of administration of such agents were disparate in the aforementioned studies.

In our previous study[19], we elucidated that p53-mediated apoptosis and growth inhibition in neural progenitor cells in the telencephalic wall occur in fetal rats following the administration of 5-FU in pregnant rats on gestational day 13. As the next step, the present study was carried out to clarify the effects and mechanisms of 5-FU on neural progenitor cells during the development of the external granule cells (EGCs) of the cerebellum as well as the cerebrum. Cerebellar granule cells have been widely used as *in vitro* models to elucidate the mechanisms of action of various therapeutic agents[14–18]. Since granule cells continue to develop after birth[20, 21], it is inferred that neonatal granule cells are highly sensitive to 5-FU. The cerebellum differs from the cerebrum in its developmental pattern, including neuronal migration and arrangement. Immature neural cells in the cerebellum develop in at least two different germinal zones; Purkinje cells and neurons originate from the ventricular zone and migrate toward the surface just beneath the molecular layer, and granular cells originate in the rhombic lip and migrate across the surface of the anlagen to the external granular layer (EGL) located just below the pia mater[20, 21]. These cells

Received: 6 January 2022, Accepted: 6 May 2022
Published online in J-STAGE: 30 May 2022
*Corresponding author: Y Yamaguchi
(e-mail: yamaguchi-yuko@bozo.co.jp)

migrate towards the deep cerebellar cortex, and finally, the cortical layer structure of the cerebellum is formed[20, 21].

Considering the characteristics of neural cells in the developing cerebellum, the present study focused on the effects of 5-FU on the EGL of the developing cerebellum, and the primary fissure of the vermis was selected as the observation area (Fig. 1). Regarding the effects of 5-FU on cerebellar granule cells in neonatal rats, only one study has reported induction of apoptosis and caspase activity; however, the analysis was performed only for 24 h, and no detailed examination of other factors was conducted[18]. To elucidate the 5-FU-induced effects and their underlying mechanism, the present study was designed to investigate changes in the morphology and immunohistochemistry to perform RT-PCR analysis of the EGCs of the developing cerebellum of six-day-old infant rats. The examination was conducted from three hours to ten days after treatment.

Materials and Methods

Animals and housing conditions

Fifteen pregnant Sprague-Dawley (Crl:CD) rats were purchased from Charles River Japan Inc. (Atsugi Breeding Center, Kanagawa, Japan) on day 13 of gestation. The date of the birth of progenies was defined as postnatal day (PND) 0. All newborn rats were separated from their dams on PND 4 and those in good health were pooled and assigned to the study. Thirteen foster mothers were selected based on their health and nursing conditions, and each mother was allowed to suckle ten infant rats. Ten infant rats from each foster mother were randomly assigned to the control group (n=5) and the 5-FU group (n=5).

All animals were housed in family units in plastic Econ cages (W 340 mm × D 450 mm × H 185 mm) with bedding (ALPHA-dri, Shepherd Specialty Papers, Inc. Richland, MI, USA) and maintained in a barrier-sustained animal room controlled at 23 ± 3°C and 50 ± 20% relative humidity, with 10 to 15 times per hour ventilation and a 12 h/12 h light/dark cycle. All dams were allowed free access to sterilized basal diet (CRF-1, Oriental Yeast Co., Ltd., Tokyo, Japan) and tap water. The experiments were carried out in accordance with the Guide for Animal Experimentation of the BoZo Research Center, Inc.

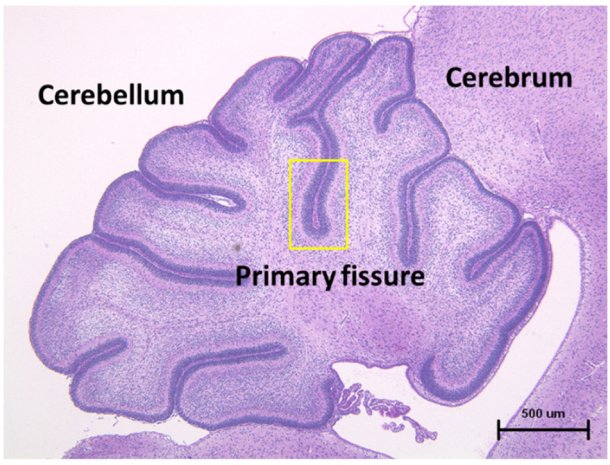

Fig. 1. Microscopic photograph of the transverse section of the normal cerebellum in a fetal rat. The external granular layer enclosed within a yellow frame in the first cleft of the central vermis was examined in the present study. Hematoxylin and eosin staining.

Chemicals

5-FU (FUJIFILM Wako Pure Chemicals, Osaka, Japan) and 5-Bromo-2'-deoxyuridine (BrdU) (Sigma-Aldrich Japan, Tokyo, Japan) were dissolved in saline solution at a dose of 40 mg/kg (10 mL/kg body weight) and 100 mg/kg (10 mL/kg body weight), respectively.

Experimental design

On PND 6, infant rats in the treatment group were injected subcutaneously with 5-FU at a dose of 40 mg/kg, and those in the control group were injected with 10 mL/kg of saline solution. The number of infant rats at each time point was each five in the control and 5-FU groups. However, after ten days of treatment, there were five rats in each group (1 dam). The dose of 5-FU was decided based on the results of our preliminary study. In the preliminary study, six-day-old rats were injected with 5-FU at doses of 30, 40, and 50 mg/kg, and the degree of apoptosis was observed in all treatment groups that were administered various doses at 9 and 24 h after treatment (HAT). The results showed that the degree of apoptosis was weak in the 30 mg/kg group. However, it was extremely severe at 9 HAT in the 50 mg/kg group. As these doses were not suitable for analyzing the time course, a dose of 40 mg/kg was selected for the present study. Infant rats in the control and 5-FU groups were euthanized at 3, 6, 12, and 24 HAT and 2, 4, and 10 d after treatment (DAT) by performing exsanguination from the abdominal aorta under isoflurane anesthesia. Half of the infant rats were subcutaneously injected with BrdU at the same time as saline or 5-FU treatment to observe the migration of EGCs, and the remaining infant rats were injected subcutaneously with BrdU 30 min before euthanasia to detect S-phase cells.

At each time point, all infant rats were dissected, and their brains were weighed. The left hemisphere of the brain was fixed in 10% buffered formalin, embedded in paraffin wax, and sectioned for histopathological and immunohistochemical examination. The right hemisphere of the cerebellum was frozen in liquid nitrogen and stored at −80°C for real-time RT-PCR analysis.

Real-time RT-PCR analysis

For real-time RT-PCR analysis, the right hemisphere of the cerebellum was acquired from five infant rats at each time point (3, 6, 12, and 24 HAT and 2 and 4 DAT) both in the control group and 5-FU group and stored at −80 °C until RNA extraction. RNA was extracted from the samples of three infant rats in both groups at each time point. Total RNA was extracted using the RNeasy Mini Kit (Qiagen,

Tokyo, Japan). First-strand cDNA was then synthesized from total RNA by reverse transcription using Taqman® Reverse Transcription Reagent (Applied Biosystems, Carlsbad, CA, USA). For real-time RT-PCR, the reaction mixture contained Power SYBR® Green PCR Master Mix (Applied Biosystems) and sense and antisense primers. The cDNA samples were preheated at 95 °C for 10 min and were subjected to 40 cycles of amplification (denaturation at 95 °C for 15 s, annealing, and extension at 60 °C for 60 s) using the StepOnePlus™ Real-Time PCR System (Applied Biosystems). PCR was performed using oligonucleotide primer sets corresponding to the cDNA sequences (p53, $p21^{cip1}$, Puma, Bax, Fas), and glyceraldehyde-3-phosphate dehydrogenase (GAPDH) was as an internal standard (Table 1).

The expression levels of mRNAs corresponding to *p53*, *p21cip1*, *Puma*, *Bax,* and *Fas* were normalized to those of the internal standard *Gadph*. The fold-changes relative to the control group values at each point are represented as the mean ± standard deviation (SD) of the values corresponding to three infants.

Histopathology

The left hemisphere of the cerebellum was trimmed longitudinally in the central vermis. The tissues were processed into paraffin-embedded blocks, sectioned at 2 μm, and stained with hematoxylin and eosin (HE).

Immunohistochemistry

Paraffin sections of the left hemisphere of the cerebellum derived from all infant rats per group at each time point were used for immunohistochemistry. Paraffin sections were deparaffinized, treated with 0.3% H_2O_2 in methanol at room temperature for 10 min, and then incubated with protein blocking buffer (Abcam, Boston, MA, USA) at room temperature for 10 min to block nonspecific reactions. Antigen retrieval was performed by heating the sections using a microwave at 95°C for 10 min in 10mM citrate buffer with a pH of 6.0. Immunohistochemistry analyses were performed for examining the expression of cleaved caspase-3 (a marker for apoptotic cells), p53, $p21^{cip1}$, phospho-histone H3 (a marker for M phase), BrdU (a marker for S phase), and calbindin, as described below.

The sections were incubated with the following primary antibodies overnight at 4 °C: rabbit anti-cleaved caspase-3 polyclonal antibody (1:200, Cell Signaling Technology, Tokyo, Japan), rabbit anti-$p21^{cip1}$ monoclonal antibody (1:100, Dako Japan, Tokyo, Japan), mouse anti-p53 polyclonal antibody (1:1,000, Santa Cruz Biotechnology, Dallas, TX, USA), rabbit anti-phospho-histone H3 polyclonal antibody (1:150, Cell Signaling Technology, Beverly, MA, USA), mouse anti-BrdU monoclonal antibody (1:200, Dako Japan), and rabbit anti-calbindin polyclonal antibody (1:800; Dako Japan). After washing, the sections were treated using the Envision+kit (Dako Japan) at room temperature for 60 min. Only for the anti-BrdU antibody, the sections were incubated with 2N HCl at room temperature for 30 min and with 0.05% protease (Protease type XXIV, Sigma-Aldrich Japan) at room temperature for 5 min before allowing to react with the primary antibody. Positive cells were visualized by performing a peroxidase-diaminobenzidine (DAB; Dojindo Laboratories, Kumamoto, Japan) reaction and counterstaining with hematoxylin.

Morphometric analysis

In HE-stained specimens, the number of pyknotic cells in the EGL at the primary fissure was counted with an upper limit of 300 cells in a field of view of 400×. The apoptosis index was calculated as the percentage of pyknotic cells among the total number of counted EGCs. The widths of the EGL and the molecular layer at the primary fissure were measured using the analytical model FlvFs-LS (Olympus, Tokyo, Japan).

In immunohistochemical specimens prepared for analyzing cleaved caspase-3, p53, $p21^{cip1}$, phospho-histone H3 in four infant rats, and BrdU in three infant rats at each time point, morphometric analyses were performed at the same site at all time points except 10 DAT. For the positive rates of each antibody without calbindin, counting and analysis were performed in the same manner as that of the apoptosis index. Calbindin-stained specimens were used to detect abnormalities in the development of Purkinje cells and dendrites in the molecular layer.

Statistical analysis

The brain weights and labeling indices (LIs%) of apoptotic EGCs and positive expression rates of cleaved caspase-3, p53, $p21^{cip1}$, phospho-histone H3, and BrdU in EGCs were expressed as the mean ± SD. The comparisons of the brain weight, widths of the EGL and molecular layer, and all labeling indices between the 5-FU and control groups at each time point were performed using the F-test, followed by a two-tailed Student's t-test and/or Welch's t-test. For all comparisons, p-values less than 5% ($p<0.05$) and 1% ($p<0.01$) were considered statistically significant.

Table 1. Oligonucleotide Primers for Each Molecule

Gene	Sense (5'-3')	Antisense (5'-3')
P53	ATATGAGCATCGAGCTCCCTCT	CACAACTGCACAGGGCATGT
P21cip1	CACGGCTCAGTGGACCAGAA	ACTGGAGCTGCCTGAGGTAGGA
Puma	ACCTCAACGCGCAGTACGAG	GGTGTCGATGTTGCTCTTCTTG
Bax	TTCATCCAGGATCGAGCAGAG	TGAGGACTCCAGCCACAAAGAT
Fas	AAGAGGAGCGTTCGTGAAACC	GATCAGCAGCCAAAGGAGCTTA
GAPDH	GCTTCACCACCTTCTTGATGTC	GAGTATGTCGTGGAGTCTACTG

Results

Clinical and macroscopic findings

No deaths occurred in dams or infant rats in any group at any time point and no noticeable clinical sign appeared. No abnormal macroscopic findings were observed in the 5-FU group at any time point during necropsy. However, the brain weights reduced significantly in the 5-FU group at 24 HAT compared to those in the control group (Fig. 2).

Results of real-time RT-PCR analysis

The expression levels of mRNAs corresponding to *p53*, *p21^{cip1}*, *Fas*, *Puma*, and *Bax* were measured by real-time RT-PCR. Among them, the expression level of *p53* mRNA significantly increased at 24 and 4 DAT and that of *p21^{cip1}* and *Fas* significantly increased at 24 HAT compared to those observed in the control group (Fig. 3). On the other hand, no significant differences were found between the control and 5-FU groups with respect to the expression levels of mRNAs corresponding to *Puma* and *Bax* throughout the experimental period (data not shown).

Histopathological and immunohistochemical findings

During the normal developmental process (Figs. 4A and 5A), the width of the EGL decreased at 10 DAT (i.e., at the age of 16 days) in the control group. In the 5-FU group (Figs. 4B and 5A), the width of the EGL decreased from 24 HAT owing to increased apoptosis of EGCs, and only a few EGCs were observed on 2 and 4 DAT. The width of the EGL at 10 DAT in the 5-FU group was comparable or slightly increased compared to that of the control group at 10 DAT. However, individual differences were observed in EGL width at 2, 4, and 10 DAT in the 5-FU group (Figs. 4B4, 4B5, and 4B6).

The apoptosis index (pyknotic EGCs) (Fig. 5B) and cleaved caspase-3-LI% (Fig. 5C) showed a similar trend; they increased gradually from 6 HAT, peaked at 24 HAT, and returned close to the control levels 2 DAT. Pyknotic EGCs were positive for cleaved caspase-3 expression (Fig. 6A–6D), and over time, changes in the cleaved caspase-3-LI% correlated well with the apoptosis index.

Although phospho-histone H3-positive mitotic EGCs were detected throughout the experimental period in the control group, the number of phospho-histone H3-positive EGCs in the 5-FU group decreased from 3 HAT, was less than 0.3% from 12 HAT to 2 DAT, and returned to the control levels observed at 4 DAT (Figs. 5D and 6E, 6F).

Few or no p21^{cip1}-positive EGCs were observed in the control group throughout the experimental period (Fig. 5E). In the 5-FU group, p21^{cip1}-LI% significantly increased at

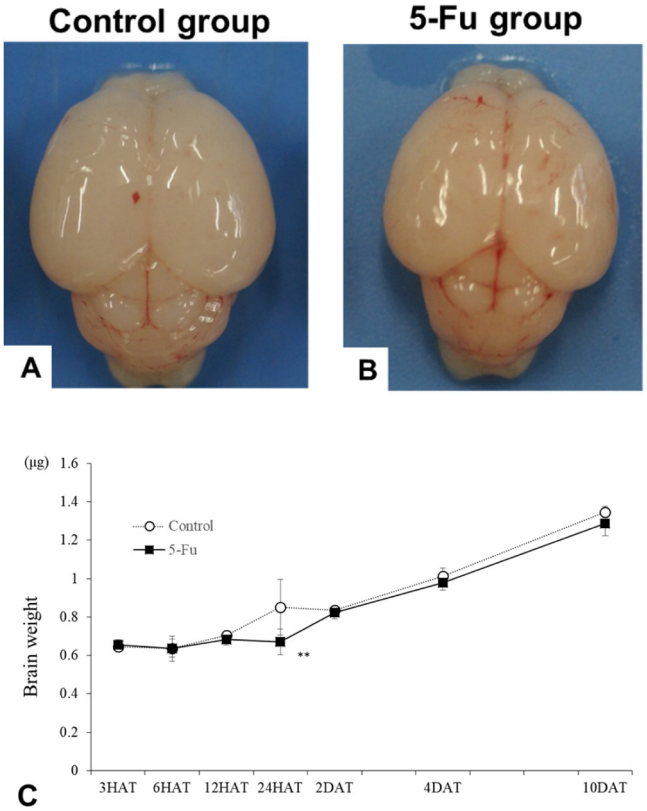

Fig. 2. (A, B) Macroscopic photograph of the brain in the control (A) and 5-FU (B) groups captured at 24 h after treatment. No changes are observed in the size and shape of the rats in the 5-FU group. (C) Changes in the brain weights were observed in the control and 5-FU groups. The brain weights in the 5-FU group decreased significantly compared to those in the control group at 24 h after treatment. *p<0.05 and **p<0.01.

24 HAT (Figs. 5E and 6G, 6H) when the cleaved caspase-3-LI% reached its maximal level (Fig. 5C).

BrdU-positive EGCs were observed at all time points in the control group (Fig. 5F). In the 5-FU group, BrdU-LI% increased at 6 and 12 HAT but decreased at 24 HAT and then returned to the control level 2 DAT (Figs. 5F and 6I, 6J).

Chronological analysis of BrdU immunohistochemistry in the control group revealed that BrdU-positive EGCs were observed on the pia mater side of the center area of EGL (Fig. 7A), on the cortical side of EGL (Fig. 7C), on the cortical side of the internal granular layer (Fig. 7E), and in the internal granular layer (Fig. 7G) at 12 and 24 HAT and 2 and 4 DAT, respectively. In contrast, BrdU-positive EGCs in the 5-FU group at 12 and 24 HAT and 2 and 4 DAT were detected on the pia mater side of EGL (Figs. 7B and 7D), in the EGL and the internal granular layer (Fig. 7F), and the internal granular layer (Fig. 7H), respectively.

Throughout the experimental period, no apparent differences were observed in the cellularity or morphology of Purkinje cells in the 5-FU group compared to that in the control group (Figs. 4 and 8).

The width of the molecular layer increased in the control group from 3 to 10 DAT along with normal development. In the 5-FU group, the molecular layer was thinner than that in the control group at 10 DAT (Figs. 4 and 9). No clear difference was observed in the number and size of Purkinje cells between the control and 5-FU groups throughout the experimental period (Fig. 4).

Discussion

In the present study, the number of pyknotic EGCs began to increase at 6 HAT and peaked at 24 HAT in the 5-FU group. Most pyknotic EGCs are immunohistochemically positive for cleaved caspase-3. The changes observed in the cleaved caspase-3-LI%, a marker of apoptosis, in the time course corresponded well to those of the aforementioned pyknotic EGCs. Therefore, the presence of pyknotic EGCs observed in this study can likely be attributed to apoptosis. It is widely known that p53 plays a crucial role in apoptosis in response to DNA damage[22–24]. Three processes have been postulated for apoptosis: induction, determination, and execution[25].

Death ligand-mediated and mitochondria-mediated pathways play major roles in the process of apoptotic determination[26–29]. The BH3-only subfamily is responsible for sensing a wide range of apoptotic stimuli and transmitting this signal to other Bcl-2 proteins to initiate apoptosis[26]. The leakage of cytochrome c from the mitochondria to the cytoplasm is determined by the balance between the expression of Bax and BH3-only proteins, such as Bid and Puma, which increase permeability, and Bcl-2 and Mcl-1 which inhibit apoptosis[27, 28]. Cytochrome c from the mitochondria binds to Apaf-1 and activates caspase-9, and caspase-9 activates caspase-3 and caspase-7[29]. In contrast, the Fas/Fas ligand activates the receptor complex (death-inducing signaling complex) and activates caspase 8, which activates the

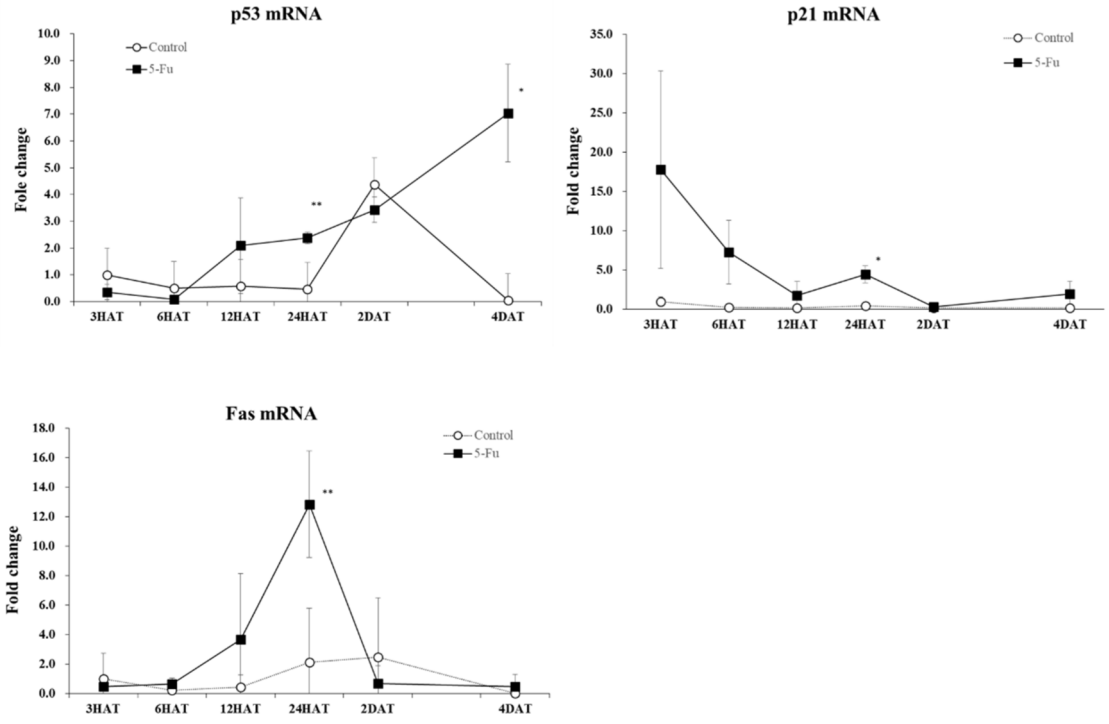

Fig. 3. Changes in the mRNA expression levels of *p53*, *p21^{cip1}*, and *Fas* in the control and 5-FU groups. In the 5-FU group, the expression level of *p53* mRNA increased at 24 h after treatment and 4 d after treatment. The expression level of *p21^{cip1}* and *Fas* mRNA increased at 24 h after treatment. *p<0.05 and **p<0.01.

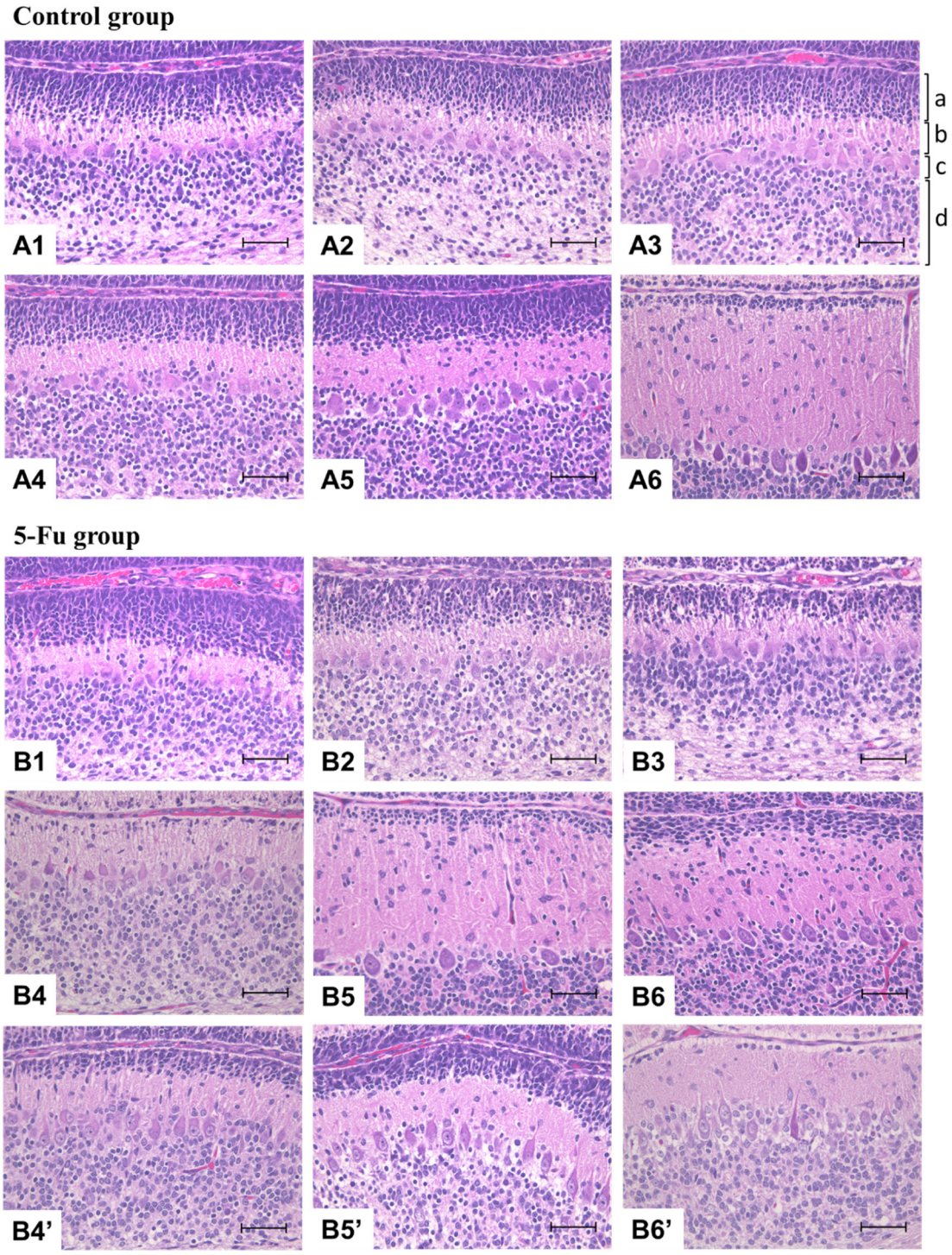

Fig. 4. Histopathological changes of the external granular layer (EGL) in the control group at 6 h after treatment (HAT) (A1), 12 HAT (A2), 24 HAT (A3), 2 d after treatment (DAT) (A4), 4 DAT (A5), and 10 DAT (A6) and in the 5-FU group at 6 HAT (B1), 12 HAT (B2), 24 HAT (B3), 2 DAT (B4), 4 DAT (B5), and 10 DAT (B6). In the 5-FU group, the width of the EGL decreased from 24 HAT to 4 DAT, and the width observed at 10 DAT was comparable to the control range or was increased slightly compared to the control group. Individual differences were observed in the width of the EGL at 2 DAT (B4'), 4 DAT (B5′), and 10 DAT (B6'). a: External granular layer, b: Molecular layer, c: Purkinje cell layer, d: Internal granular layer. Hematoxylin and eosin staining. Bar: 100 μm.

lower caspases 3 and 7 involved in the execution[30].

p53 may be responsible for 5-FU-induced apoptosis in human cancer cells[31–33]. However, since the expression of p53 varies in cancer cells, it is unclear whether its expression and mechanism are the same as those observed in normal EGCs. Esperanza et al. reported that 5-FU-induced

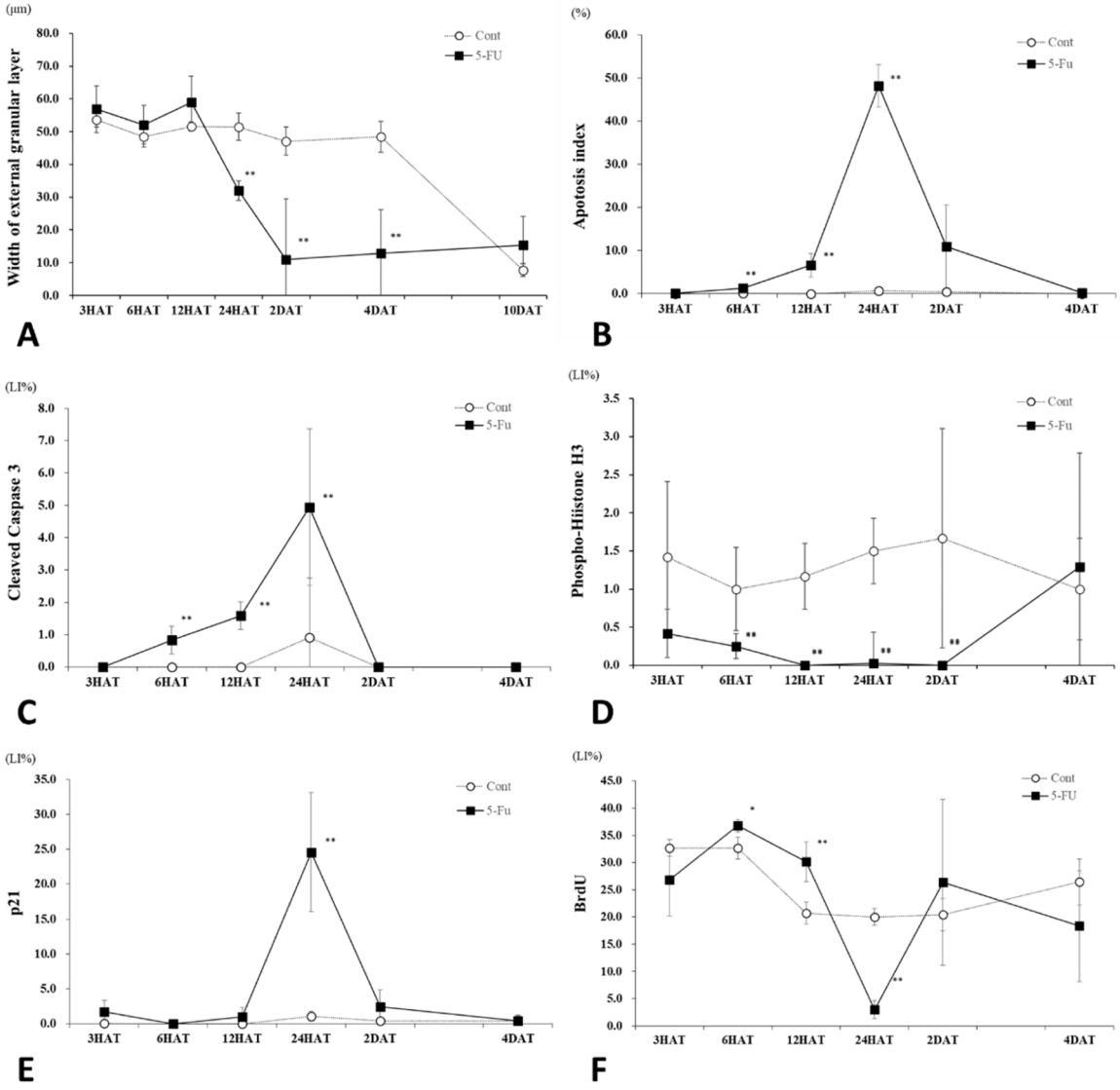

Fig. 5. (A) Changes in the width of the external granular layer (EGL) in the control and 5-FU groups. In the 5-FU group, the width of the EGL significantly decreased from 24 h after treatment (HAT) to 4 d after treatment (DAT) compared to the control group. (B) Changes in the apoptotic external granular cells (EGCs) in the control and 5-FU groups. In the 5-FU group, the apoptosis index increased gradually from 6 HAT, peaked at 24 HAT, and returned close to the control levels at 2 DAT. (C) Changes in the cleaved caspase-3-LI% of EGCs in the control and 5-FU groups. In the 5-FU group, the index increased gradually from 6 HAT, peaked at 24 HAT, and returned close to the control levels at 2 DAT. (D) Changes in the phospho-histone H3-LI% of EGCs in the control and 5-FU groups. In the 5-FU group, the index decreased significantly from 6 HAT to 2 DAT and returned to the control value at 4 DAT. (E) Changes in the $p21^{cip1}$-LI% of EGCs in the control and 5-FU groups. In the 5-FU group, the index increased significantly at 24 HAT. (F) Changes in the BrdU-LI% of EGCs in the control and 5-FU groups. In the 5-FU group, the index increased significantly at 6 and 12 HAT, decreased at 24 HAT, and returned to the control value at 2 DAT. *$p<0.05$ and **$p<0.01$.

apoptosis of the cells of the normal thymus in mice is associated with the co-expression of Fas, Bax, and caspase-3[34]. Apoptosis of granule cells in the cerebellum after intraperitoneal administration of 5-FU to seven-day-old rats has been attributed to the activation of the apoptotic pathway of caspase-3[18]. In the present study, real-time RT-PCR analysis revealed that the expression levels of p53 at 24 HAT and 4 DAT and Fas at 24 HAT increased significantly in the 5-FU group, whereas no difference in the expression levels of *Puma* and *Bax* was detected between the control and 5-FU groups at any time point. These results are almost the same as those presented in the aforementioned reports, indicating that apoptosis is not mediated by the mitochondrial pathway and that Fas-activated caspase-8 activates caspase-3, resulting in apoptosis without involving the mitochondrial pathway. The reason for high levels of p53 expression observed at 4 DAT in the 5-FU group and the role of p53 in the apoptosis of EGCs under present experimental conditions have not been clarified.

In the 5-FU group, phospho-histone H3-LI% was sig-

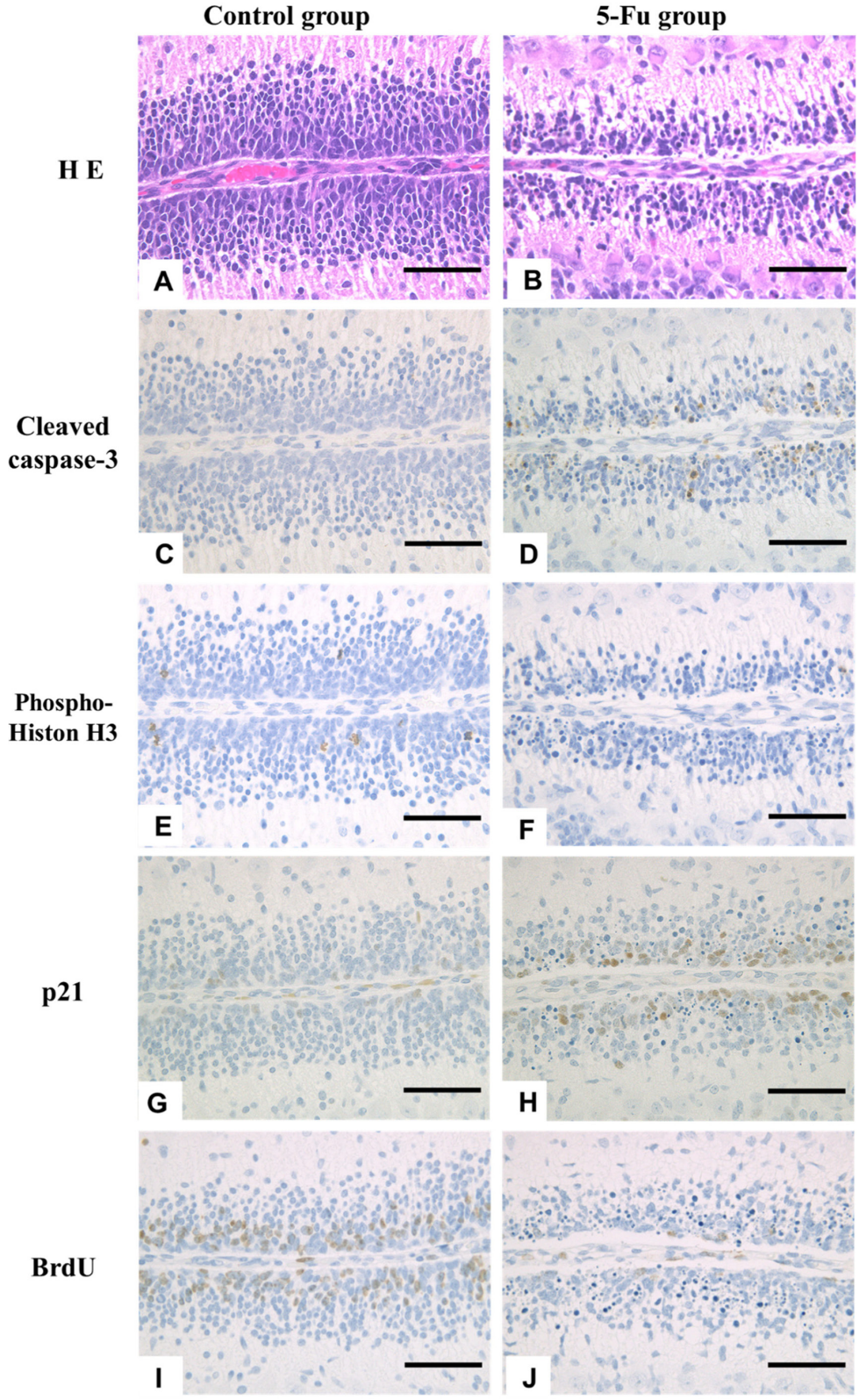

Fig. 6. (A–D) Microscopic photograph of external granular layer (EGL) stained with Hematoxylin and Eosin and cleaved caspase-3 expression at 24 h after treatment (HAT) in the control and 5-FU groups. Increased pyknotic external granular cells (EGCs) were observed in the 5-FU group (B). Pyknotic EGCs were positive for the expression of cleaved caspase-3 (D). (E–J) Immunohistochemical expression of phospho-Histone H3, $p21^{cip1}$, and BrdU at 24 HAT in the control (E, G, and I) and 5-FU (F, H, and J) groups. In the 5-FU group, a few phospho-histone H3- and BrdU-positive EGCs were detected (F and J), and the number of $p21^{cip1}$-positive EGCs increased (H) compared to the control group. The rats were injected with BrdU 30 min before euthanasia to detect S phase cells. Hematoxylin and eosin stain and Immunostaining. Bar: 100 µm.

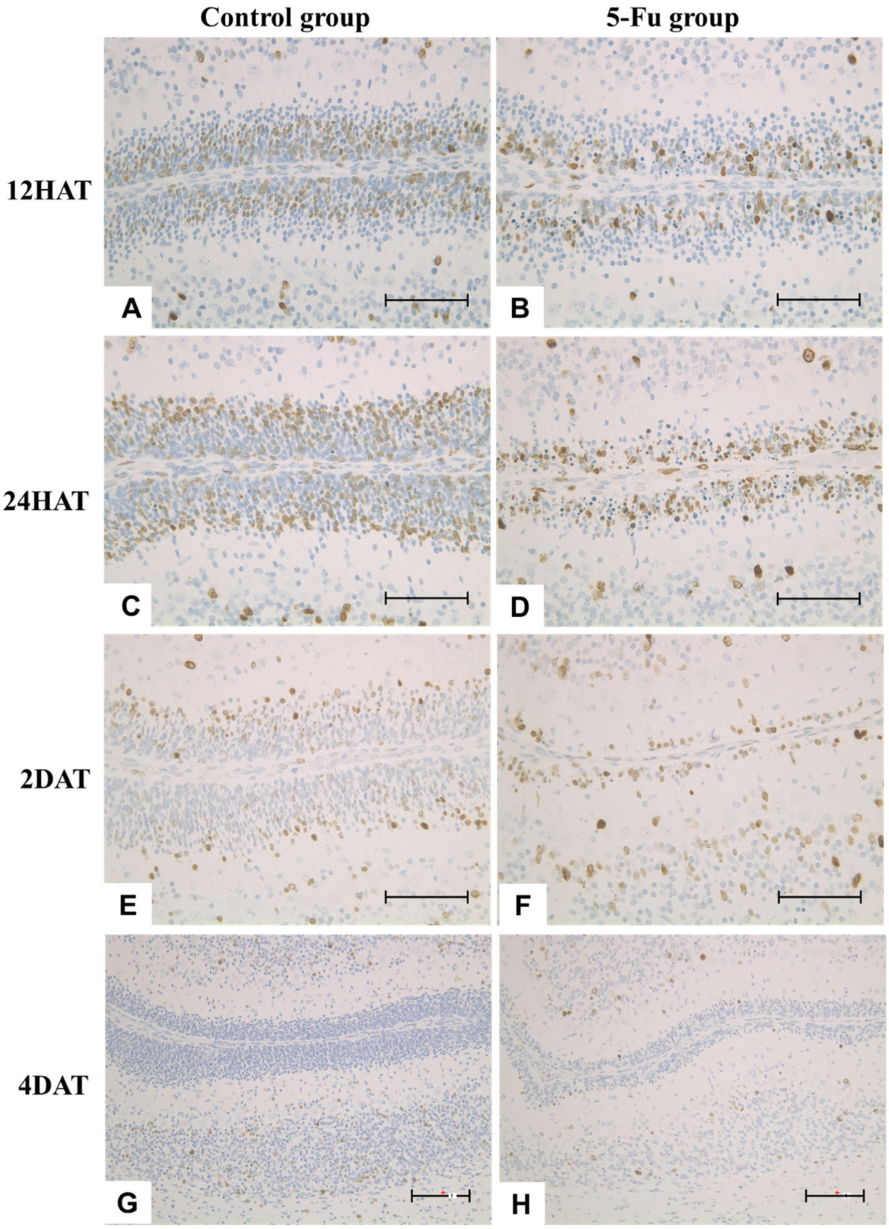

Fig. 7. (A–H) Immunohistochemical expression of BrdU at 12 h after treatment (HAT), 24 HAT, 2 DAT, and 4 d after treatment (DAT) in the control (A, C, E, and G) and 5-FU (B, D, F, and H) groups. In the control group, BrdU-positive external granular cells (EGCs) were located on the pia mater side to the center area of the external granular layer (EGL) (A), on the cortical side of EGL (C), on the cortical side of the internal granular layer (E), and in the internal granular layer (G) at 12 HAT, 24 HAT, 2 DAT, and 4 DAT respectively. In the 5-FU group, BrdU- positive EGCs were located on the pia mater side of EGL (B, D), in the external and internal granular layer (F), and in the internal granular layer at 12 and 24 HAT, 2 DAT, and 4 DAT, respectively. The rats were injected with BrdU at the same time as saline or 5-FU treatment to observe the migration of EGCs. Immunostaining. Bar: 100 µm.

nificantly decreased at 6 and 12 HAT and 2 DAT, and BrdU-LI% was significantly decreased at 24 HAT. In contrast, the cleaved caspase-3-LI%, indicating the apoptosis index, increased from 6 HAT, peaked at 24 HAT, and returned to control levels at 2 DAT. These results indicate that 5-FU not only induces apoptosis but also suppresses cell proliferative activity, resulting in a reduction in the width of the external granular layer and brain weight.

It is well known that the expression of p53 is induced by DNA damage and various stresses. It functions as a transcriptional activator in the nucleus and plays a crucial role in cell cycle arrest, induction of apoptosis, and DNA repair. Furthermore, p53 is activated in cells with DNA damage, resulting in cell cycle arrest in G1 and G2/M phases. During this period, it inhibits DNA mutation by facilitating DNA repair[35]. P21 is a downstream target of p53 and a potent cyclin-dependent kinase inhibitor that functions as a regulator of cell cycle progression in the G1-S and M

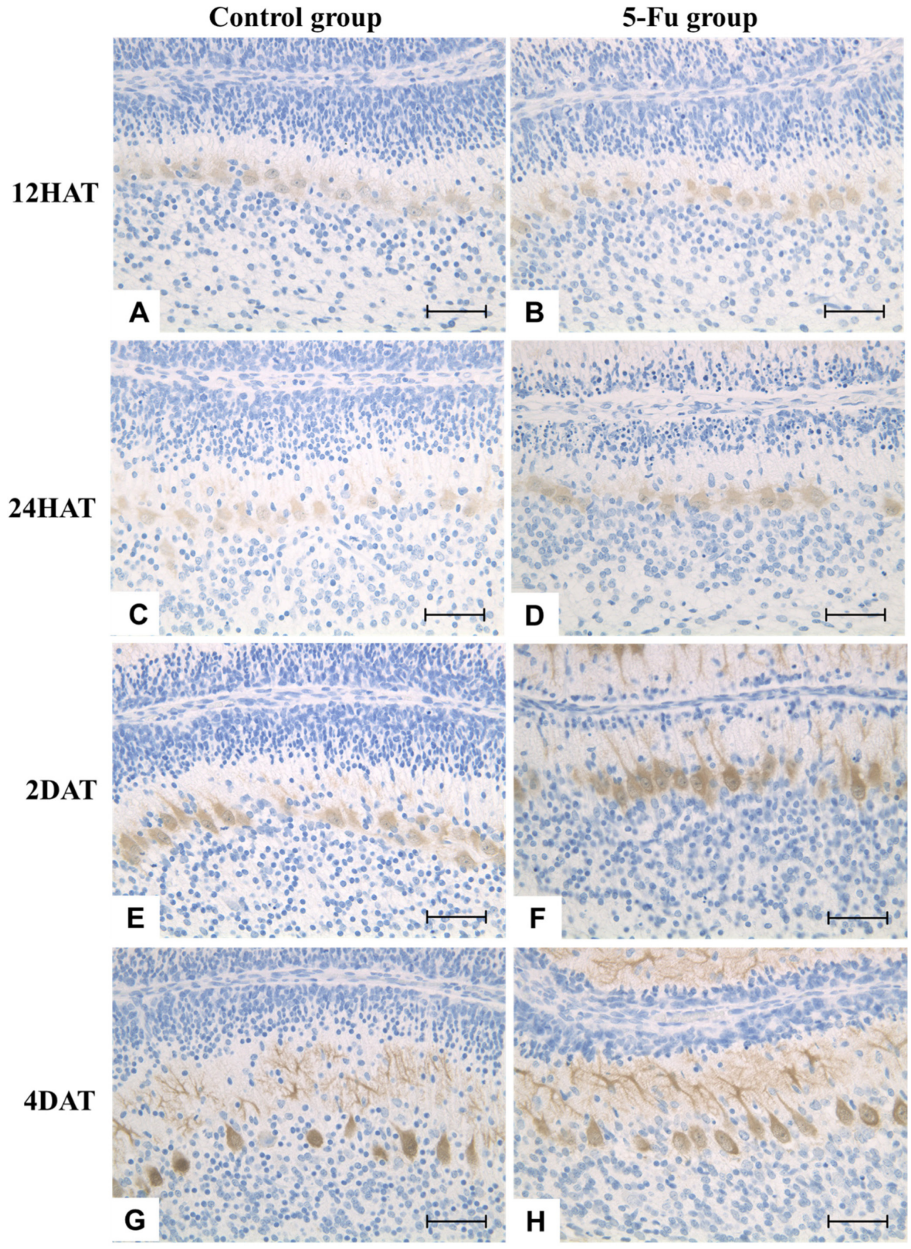

Fig. 8. (A–H) Immunohistochemical expression of calbindin at 12 h after treatment (HAT), 24 HAT, 2 d after treatment (DAT), and 4 DAT in the control (A, C, E, and G) and 5-FU (B, D, F, and H) groups. Throughout the experimental period, no notable differences in the cellularity or morphology of Purkinje cells were observed in the 5-FU group compared to those in the control group. The somatic size of Purkinje cells progressively increased by 2 DAT (eight-day-old rats). Dendritic development was observed at 4 DAT (ten-day-old rats). Immunostaining. Bar: 100 µm.

phases[36–38]. BrdU-LI% was increased at 6 and 12 HAT, but $p21^{cip1}$-LI% significantly increased at 24 HAT when BrdU-LI% decreased. In addition, real-time RT-PCR analysis revealed that the expression levels of mRNAs corresponding to *p53* and *p21cip1* were significantly increased at 24 HAT. Shuey *et al.*[3, 4] reported that 5-FU induced an increase in the number of S-phase cells at 8 HAT and a remarkable decrease at 24 HAT in the liver of fetal rats, and the peak in the inhibition of TS activity observed in the liver at 24 HAT may be attributed to these cell cycle effects. In the present study, an increase of BrdU-positive S phase cells at the early time points, as described in the aforementioned reference, is likely to reflect the accumulation of S phase cells (late G1 phase cells) until 24 HAT, when a peak of the inhibition of TS activity was observed. These results suggest that 5-FU induced p53-dependent accumulation of cells in the S phase and arrest of EGCs in the G1-S and G2-M phase, resulting in a reduction in the number of mitotic and S phase cells observed in the present study.

The similarities between changes observed in the 5-FU

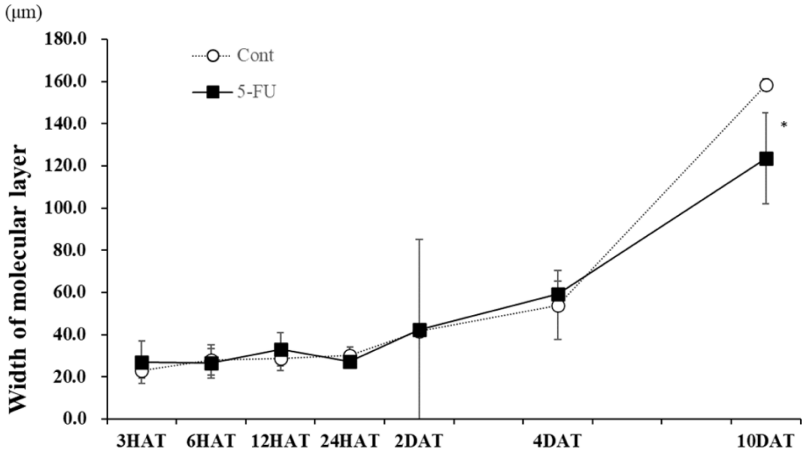

Fig. 9. Changes in the width of the molecular layer in the control and 5-FU groups. In the 5-FU group, the width of the molecular layer decreased at 10 d after treatment compared to the control group.

group in the present study and those observed in our previous study[19] investigating the effects of 5-FU in neural progenitor cells in the fetal telencephalic wall are outlined as follows: (1) mitosis was remarkably reduced, and G2-M phase arrest occurred from the early stages of treatment followed by apoptosis and G1-S phase arrest; (2) cell proliferative activity was reduced due to a decrease in the number of S phase cells. Some differences in the changes observed in the 5-FU group in these two studies were also noted. In a previous study, the apoptosis index of the neural progenitor cells of the telencephalic wall that were treated with 5-FU showed high values from 9 HAT to 24 HAT and then gradually decreased, strongly suggesting that apoptosis was mediated by p53 because the p53-LI% was significantly higher in the 5-FU group prior to apoptosis. In the present study, the apoptosis index in EGCs treated with 5-FU increased gradually from 6 HAT, peaked at 24 HAT, and then decreased sharply at 2 DAT. However, p53 levels were not significantly higher in the 5-FU group in the present study prior to apoptosis, and the association between apoptosis and p53 expression was not clear. In addition, here, S-phase accumulation was observed at 6 and 12 HAT in the 5-FU group. These differences indicate that 5-FU-induced apoptosis in EGCs was less severe than that observed in neural progenitor cells of the telencephalic wall and that cellular arrest was more apparent in EGCs. Thus, such differences in the degree and duration of apoptosis and the association between apoptosis and p53 are likely to be attributed to the differences in fetal and neonatal exposure to treatment that was administered via different routes and at varying doses in these two studies.

No difference was observed in the development of Purkinje cells between the 5-FU and control groups at any time point. Bejar *et al.* reported that changes in Bergmann glial cells induced by the mitochondrial inhibitor, methylazoxymethanol, were drastic in mice when they were treated at an age of 0 days, whereas the structure was maintained in mice treated at an age of 5 days. They speculated that this difference was due to the date of the treatment. Purkinje cells undergo complete terminal differentiation from day 10 to 13 of gestation and migrate to the cerebellar cortex (parenchyma) by day 16 or 17 of gestation. After birth, cell bodies develop until nine days and dendrites develop rapidly after nine days[39]. Therefore, at the time of administration in this study (six-day-old rats), it is conceivable that Purkinje cells were not affected by 5-FU treatment because they were already in the stage of cell body development and had no proliferative activity.

A few BrdU (simultaneous administration)-positive cells in the inner granular layer observed 4 DAT are likely to reflect the migration of surviving EGCs into the inner granular layer. Therefore, under the experimental conditions of our study, it is likely that 5-FU did not affect the migration of external granule cells. However, because the width of the molecular layer in the 5-FU group was thinner at 10 DAT, the effect of 5-FU in the molecular layer may become clearer as time progresses.

At 10 DAT, the width and cell density of the external and internal granular layers in some 5-FU-treated rats were similar to those of the control group. This finding suggests that remarkable regeneration of granule cells can be observed between 4 and 10 DAT (10–16 days of age) and is a crucial event. In contrast, the reason for the increased expression of *p53* mRNA observed at 4 DAT is unclear; however, this fluctuation may reflect events observed in other areas of the cerebellum.

In conclusion, this study elucidated the changes observed in the time-course of EGCs in the vermis of the cerebellum after a single subcutaneous administration of 5-FU to six-day-old infant rats. 5-FU induced the apoptosis of EGCs by activating the Fas and caspase-3 pathways without involving the mitochondrial pathway and led to the p53-dependent accumulation of cells in the S phase, thereby leading to G1-S and G2-M phase arrest. This finding indicates that 5-FU inhibited the proliferative activity of EGCs. EGCs recovered remarkably from 4 to 10 DAT. Further-

more, 5-FU, when administered at an age of six days, may not affect the development of Purkinje cells or migration of EGCs. Although it is well known that 5-FU induces apoptosis in normal and cancer cells, the mechanisms are not the same and are poorly understood[18, 31–34]. This study provides useful information for elucidating the mechanisms underlying CNS malformations, adult neurotoxicity, and p53-independent apoptosis in human cancer cells induced by 5-FU.

Disclosure of Potential Conflicts of Interest: The authors declare no conflicts of interest directly relevant to the content of this article.

Acknowledgments: We are grateful to Dr. Kunitoshi Mitsumori, Professor Emeritus of the Tokyo University of Agriculture and Technology, for his critical review of this manuscript. We also thank Ms. Momoko Ikeya and Tomomi Yoshimoto, BoZo Research Center, Inc., for the immunohistochemical staining.

References

1. Longley DB, Harkin DP, and Johnston PG. 5-fluorouracil: mechanisms of action and clinical strategies. Nat Rev Cancer. **3**: 330–338. 2003. [Medline] [CrossRef]
2. Inoue T, and Horii I. Effects on fetal thymocyte populations and postnatal T-cell-dependent immune functions after maternal exposure to 5-fluorouracil during pregnancy in mice. J Toxicol Sci. **27**: 79–86. 2002. [Medline] [CrossRef]
3. Shuey DL, Lau C, Logsdon TR, Zucker RM, Elstein KH, Narotsky MG, Setzer RW, Kavlock RJ, and Rogers JM. Biologically based dose-response modeling in developmental toxicology: biochemical and cellular sequelae of 5-fluorouracil exposure in the developing rat. Toxicol Appl Pharmacol. **126**: 129–144. 1994. [Medline] [CrossRef]
4. Shuey DL, Setzer RW, Lau C, Zucker RM, Elstein KH, Narotsky MG, Kavlock RJ, and Rogers JM. Biological modeling of 5-fluorouracil developmental toxicity. Toxicology. **102**: 207–213. 1995. [Medline] [CrossRef]
5. Lau C, Mole ML, Copeland MF, Rogers JM, Kavlock RJ, Shuey DL, Cameron AM, Ellis DH, Logsdon TR, Merriman J, and Setzer RW. Toward a biologically based dose-response model for developmental toxicity of 5-fluorouracil in the rat: acquisition of experimental data. Toxicol Sci. **59**: 37–48. 2001. [Medline] [CrossRef]
6. Paskulin GA, Gazzola Zen PR, de Camargo Pinto LL, Rosa R, and Graziadio C. Combined chemotherapy and teratogenicity. Birth Defects Res A Clin Mol Teratol. **73**: 634–637. 2005. [Medline] [CrossRef]
7. Hanaoka H, Kubota T, Matsui K, Kadokura Y, Iida M, Yamada Y, and Moteki H. A case of leukoencephalopathy after drip infusion of 5-fluoroirasil (in Japanese). Pract Odontol. **109**: 161–163. 2002.
8. Leyder M, Laubach M, Breugelmans M, Keymolen K, De Greve J, and Foulon W. Specific congenital malformations after exposure to cyclophosphamide, epirubicin and 5-fluorouracil during the first trimester of pregnancy. Gynecol Obstet Invest. **71**: 141–144. 2011. [Medline] [CrossRef]
9. Bourke RS, West CR, Chheda G, and Tower DB. Kinetics of entry and distribution of 5-fluorouracil in cerebrospinal fluid and brain following intravenous injection in a primate. Cancer Res. **33**: 1735–1746. 1973. [Medline]
10. Han R, Yang YM, Dietrich J, Luebke A, Mayer-Pröschel M, and Noble M. Systemic 5-fluorouracil treatment causes a syndrome of delayed myelin destruction in the central nervous system. J Biol. **7**: 12. 2008. [Medline] [CrossRef]
11. Doi K. Mechanisms of neurotoxicity induced in the developing brain of mice and rats by DNA-damaging chemicals. J Toxicol Sci. **36**: 695–712. 2011. [Medline] [CrossRef]
12. Bejar A, Roujansky P, de Barry J, and Gombos G. Different effect of methylazoxymethanol on mouse cerebellar development depending on the age of injection. Exp Brain Res. **57**: 279–285. 1985. [Medline] [CrossRef]
13. Ohmori H, Ogura H, Yasuda M, Nakamura S, Hatta T, Kawano K, Michikawa T, Yamashita K, and Mikoshiba K. Developmental neurotoxicity of phenytoin on granule cells and Purkinje cells in mouse cerebellum. J Neurochem. **72**: 1497–1506. 1999. [Medline] [CrossRef]
14. Fritsch P, Richard-Le Naour H, Denis S, and Ménétrier F. Kinetics of radiation-induced apoptosis in the cerebellum of 14-day-old rats after acute or during continuous exposure. Int J Radiat Biol. **66**: 111–117. 1994. [Medline] [CrossRef]
15. Pisu MB, Roda E, Guioli S, Avella D, Bottone MG, and Bernocchi G. Proliferation and migration of granule cells in the developing rat cerebellum: cisplatin effects. Anat Rec A Discov Mol Cell Evol Biol. **287**: 1226–1235. 2005. [Medline] [CrossRef]
16. Sugiyama A, Sun J, Ueda K, Furukawa S, and Takeuchi T. Effect of methotrexate on cerebellar development in infant rats. J Vet Med Sci. **77**: 789–797. 2015. [Medline] [CrossRef]
17. Ohira T, Ando R, Saito T, Yahata M, Oshima Y, and Tamura K. Busulfan-induced pathological changes of the cerebellar development in infant rats. Exp Toxicol Pathol. **65**: 789–797. 2013. [Medline] [CrossRef]
18. Zhang Y, Yin N, Liang S, Shen S, Li D, and Faiola F. 5-fluorouracil-induced neurotoxicity in rat cerebellum granule cells involves oxidative stress and activation of caspase-3 pathway. Int J Clin Exp Med. **12**: 2334–2343. 2019.
19. Yamaguchi Y, Fukunaga Y, Takagi M, Saito T, Tamura K, and Hoshiya T. Time-course changes in 5-fluorouracil-induced neural progenitor cell damages in the developing rat brain. J Toxicol Pathol. **34**: 299–308. 2021. [Medline] [CrossRef]
20. Chizhikov V, and Millen KJ. Development and malformations of the cerebellum in mice. Mol Genet Metab. **80**: 54–65. 2003. [Medline] [CrossRef]
21. Leto K, Arancillo M, Becker EB, Buffo A, Chiang C, Ding B, Dobyns WB, Dusart I, Haldipur P, Hatten ME, Hoshino M, Joyner AL, Kano M, Kilpatrick DL, Koibuchi N, Marino S, Martinez S, Millen KJ, Millner TO, Miyata T, Parmigiani E, Schilling K, Sekerková G, Sillitoe RV, Sotelo C, Uesaka N, Wefers A, Wingate RJ, and Hawkes R. Consensus paper: cerebellar development. Cerebellum. **15**: 789–828. 2016. [Medline] [CrossRef]
22. Uberti D, Belloni M, Grilli M, Spano P, and Memo M. Induction of tumour-suppressor phosphoprotein p53 in the apoptosis of cultured rat cerebellar neurones triggered by excitatory amino acids. Eur J Neurosci. **10**: 246–254. 1998. [Medline] [CrossRef]

23. Lakin ND, and Jackson SP. Regulation of p53 in response to DNA damage. Oncogene. **18**: 7644–7655. 1999. [Medline] [CrossRef]
24. Oren M. Decision making by p53: life, death and cancer. Cell Death Differ. **10**: 431–442. 2003. [Medline] [CrossRef]
25. Zhang X-P, Liu F, and Wang W. Two-phase dynamics of p53 in the DNA damage response. Proc Natl Acad Sci USA. **108**: 8990–8995. 2011. [Medline] [CrossRef]
26. Tsujimoto Y. Role of Bcl-2 family proteins in apoptosis: apoptosomes or mitochondria? Genes Cells. **3**: 697–707. 1998. [Medline] [CrossRef]
27. Leibowitz B, and Yu J. Mitochondrial signaling in cell death via the Bcl-2 family. Cancer Biol Ther. **9**: 417–422. 2010. [Medline] [CrossRef]
28. Yu J, and Zhang L. PUMA, a potent killer with or without p53. Oncogene. **27**(Suppl 1): S71–S83. 2008. [Medline] [CrossRef]
29. Brentnall M, Rodriguez-Menocal L, De Guevara RL, Cepero E, and Boise LH. Caspase-9, caspase-3 and caspase-7 have distinct roles during intrinsic apoptosis. BMC Cell Biol. **14**: 32. 2013. [Medline] [CrossRef]
30. Cryns V, and Yuan J. Proteases to die for. Genes Dev. **12**: 1551–1570. 1998. [Medline] [CrossRef]
31. Motamedi Z, Amini SA, Raeisi E, Lemoigne Y, and Heidarian E. Combined effects of protocatechuic acid and 5-fluorouracil on p53 gene expression and apoptosis in gastric adenocarcinoma cells. Turk J Pharm Sci. **17**: 578–585. 2020. [Medline] [CrossRef]
32. Satari A, Amini SA, Raeisi E, Lemoigne Y, and Heidarian E. Synergetic impact of combined 5-fluorouracil and rutin on apoptosis in PC3 cancer cells through the modulation of P53 gene expression. Adv Pharm Bull. **9**: 462–469. 2019. [Medline] [CrossRef]
33. Hou J, Tan Y, Su C, Wang T, Gao Z, Song D, Zhao J, Liao Y, Liu X, Jiang Y, Feng Q, Wan Z, and Yu Y. Inhibition of protein FAK enhances 5-FU chemosensitivity to gastric carcinoma *via* p53 signaling pathways. Comput Struct Biotechnol J. **18**: 125–136. 2019. [Medline] [CrossRef]
34. Aquino Esperanza JA, Aguirre MV, Aispuru GR, Lettieri CN, Juaristi JA, Alvarez MA, and Brandan NC. In vivo 5-fluorouracil-[corrected]induced apoptosis on murine thymocytes: involvement of FAS, Bax and Caspase3. Cell Biol Toxicol. **24**: 411–422. 2008. [Medline] [CrossRef]
35. Vogelstein B, and Kinzler KW. Cancer genes and the pathways they control. Nat Med. **10**: 789–799. 2004. [Medline] [CrossRef]
36. el-Deiry WS, Tokino T, Velculescu VE, Levy DB, Parsons R, Trent JM, Lin D, Mercer WE, Kinzler KW, and Vogelstein B. WAF1, a potential mediator of p53 tumor suppression. Cell. **75**: 817–825. 1993. [Medline] [CrossRef]
37. Zhang XP, Liu F, and Wang W. Coordination between cell cycle progression and cell fate decision by the p53 and E2F1 pathways in response to DNA damage. J Biol Chem. **285**: 31571–31580. 2010. [Medline] [CrossRef]
38. Bunz F, Dutriaux A, Lengauer C, Waldman T, Zhou S, Brown JP, Sedivy JM, Kinzler KW, and Vogelstein B. Requirement for p53 and p21 to sustain G2 arrest after DNA damage. Science. **282**: 1497–1501. 1998. [Medline] [CrossRef]
39. McKay BE, and Turner RW. Physiological and morphological development of the rat cerebellar Purkinje cell. J Physiol. **567**: 829–850. 2005. [Medline] [CrossRef]